 doi:10.20944/preprints202206.0416.v1

Article

Surface and Electrical Characterization of Bilayers Based on $Bifeo_3$ and Vo_2

J. Martínez [1], E. Mosquera-Vargas [1,2,*], V. Fuenzalida [3], M. Flores [3], G. Bolaños [4,*] and J. E. Diosa [1,2,*]

[1]Grupo de Transiciones de Fase y Materiales Funcionales, Departamento de Física, FCNE, Universidad del Valle, Santiago de Cali, Colombia.
[2] Centro de Excelencia en Nuevos Materiales (CENM), Universidad del Valle, Santiago de Cali, Colombia.
[3]Laboratorio de Superficies y Nanomateriales, Departamento de Física, FCFM, Universidad de Chile, Av. Blanco Encalada 2008, Santiago de Chile, Chile
[4] Grupo de Física de Bajas Temperaturas, Universidad del Cauca, Popayán, Colombia

ABSTRACT

Thin films of $BiFeO_3$ (BFO), VO_2 and BFO/VO_2 were grown on $SrTiO_3(100)$ and $Al_2O_3(0001)$ monocrystalline substrates using the RF and DC sputtering techniques. The surface of the films was characterized by profilometry, AFM and XPS. The heterostructures have roughnesses between 0.2 and 16 nm and a grain size between 20 nm and 67 nm. XPS measurements show a higher proportion of the V^{4+} and Bi^{3+} oxides. In the Fe region, a higher proportion of Fe^{3+} is shown in the films. The homogeneous ordering, low roughnesses and the oxidation states on the obtained surface show a good coupling in these films. The I-V curves show ohmic behavior at room temperature and change with increasing temperature. The effect of coupling these materials in a thin film shows the appearance of hysteresis cycles I-V and R-T, typical of materials with high potential in applications such as resistive memories and solar cells.

Keywords: Thin films; $BiFeO_3/VO_2$; Solid-solid interface; Surface characterization; Electrical property

1. Introduction

Bismuth ferrite ($BiFeO_3$ (BFO)), is a multiferroic materials exhibiting coexistence of ferroelectricity (FE) and antiferromagnetism (AF) at room temperature [1]–[5]. In thin film form, the FE and AF order parameters of multiferroics could be affected for the phenomenon of magnetostriction [1]–[4] due to the change in the dimensions of the material as a consequence of stresses generated at the contact interface, either with the substrate or with another material. To study this mechanism of coupling at the interface with BFO, the vanadium dioxide (VO_2) system was used, which has been widely analyzed due to the structural change it undergoes from VO_2 (monoclinic) to VO_2 (tetragonal) at a temperature of 340 K, showing weak ferromagnetic behavior [6], [7]. The combination of these materials in heterostructures gives access to the study of mixed properties and their control.

 doi:10.20944/preprints202206.0416.v1

As far as we can determine, there are currently no reports in the literature that show the growth of BFO thin films over VO_2. This is mainly due to the incompatibility between the crystalline structures analyzed. However, there are reports on the growth of bilayers with similar crystalline structures or lattice parameters close to those of BFO and VO_2 that presented good coupling, compatibility and interesting physical properties, such as the TiO_2 and de $BaTiO_3$. Good compatibility might therefore be expected in the bilayer system based on BFO and VO_2 since the interface effects are predominant and detectable in analogous materials [8]. de la Venta et al, [6], [7], [9], [10] showed the change in the coercivity of thin films of nickel deposited on V_2O_3 and VO_2, a change attributed to the structural phase transition of V_2O_3 and VO_2. Saerbeck et al, [11] studied and compiled information about the coupling between magnetism and the structural phase transition by interfacial tension in different systems of $La_{0.7}A_{0.3}MnO_3$ (A = Sr,Ca), Fe_3O_4, $CoFe_2O_4$, FeRh, Ni, Fe and Co, using as a base the structural change in the VO_2, V_2O_3 and $BaTiO_3$ compounds, resulting in structures with hybrid properties that manage to modify and/or control the magnetic behavior through effects of tension and inverse magnetostriction. A recent study [12] reports the progress in BFO-based superlattices, which the physical properties of these multifunctional materials have not been explored enough.

On the other hand, Lee et al [13] reported that the $BaTiO_3$ presents a perovskite-type crystalline structure like that of $BiFeO_3$ with magnetostriction effects. They report on the modification of the tension of $SrRuO_3$ and $La_{0.67}Sr_{0.33}MnO_3$ films induced by the phase transition of $BaTiO_3$ substrate, observing the effects that a biaxial stress induces on the electric and magnetic transport of these compounds.

Furthermore, Burbure et al, [14] studied the orientation and phase relationship between TiO_2 films and $BaTiO_3$ substrates, considering that TiO_2 has structure and lattice parameters of VO_2, they determined that despite having a high mismatch index, bilayers that present good coupling and epitaxy were grown in different crystalline planes. Feng [15] and Sarkar et al [16], worked on the development of multifunctional nano-heterostructures of $BiFeO_3/TiO_2$, analyzing photo-ferroelectricity, transport, and non-volatile switching resistances. Zhang et al [17], used combinatorial substrate epitaxy (CSE) in 150 samples, for the determination of the phase and orientation relationships in $BiFeO_3/TiO_2$ bilayers. They also proposed the configuration scheme structure whereby the coupling between the layers of these materials with mismatch is presented. However, it was shown that the structural coupling of both the anatase phase of TiO_2 (like VO_2 (M)) and the rutile phase (like VO_2 (R)) is ordered.

This paper deals with the growth of BFO thin films previously coated with VO_2. We report on surface analysis of single material and bilayers films, their growth rate, roughness, and grain size. In addition, an electrical study was carried out.

 doi:10.20944/preprints202206.0416.v1

2. Experimental details

Thin films of BFO, VO_2 and BFO/VO_2 were grown on $SrTiO_3$(100) and Al_2O_3(0001) substrates using RF and DC sputtering under internal pressure of 4.5 x 10^{-4} mbar and atmospheres of argon and oxygen. All materials, targets (BFO and metallic vanadium, V, with purity ≥ 99.99 %), and substrates, were obtained from Plasmaterials, Inc. The VO_2 films were grown in an O_2-atmosphere at a pressure of 1.72 mbar, power of 53 W, and substrate temperature of 450° C. In turn, the top BFO layer was deposited in an argon atmosphere (2 x 10^{-1} mbar) at a power of 100 W and a substrate temperature of 550° C. After deposition, both the single VO_2 films and the heterostructures were annealed in-situ for 20 minutes in 20 % of O_2 and 80 % of Ar mixed atmosphere (p = 2.4 x 10^{-1} mbar) at the same growth temperature of 550 °C. Monolayers of BFO and VO_2 with "steps" were obtained, covering a section of the substrate with an alumina mask, thus allowing the deposition of the material only in one region of the substrate.

Contact profilometry measurements were performed using a KLA Tencor D-120 equipment with a measuring range from 1 nm to 100 µm, to determine the thickness of the thin films and their growth rate. The surface morphology of the films was examined with an atomic force microscope (AFM, Omicron SPM1) and the Gwyddion software was used to determine the statistical parameters of roughness. The images were processed with an adjusted linear plane, to eliminate the inclination before the statistical analysis. Average grain diameter was obtained using ImageJ software. This software was used to delineate the perimeter of the grain assuming a circular surface. The elemental composition of the films and the resolution spectra were studied by means of X-ray photoelectron spectroscopy (XPS) using a multi-technique scanning XPS microprobe (PHI Versa Probe II). The source of X-rays used was a monochromatic AlKα lamp (300 W) at a photon energy of 2.38 x 10^{-16} J. The photoelectron detection was carried out by means of a concentric hemispherical analyzer (CHA) (PHI 10360 Model) operating with an analytical aperture 0.8 m in diameter. The binding energy resolution of the instrument is 1.12 x 10^{-19} J, with Kα radiation unfiltered from an Al (hγ = 1486.6 eV) anode, with a measurement step of 0.5 eV. The XPS spectra were adjusted using the Multipack and XPSpeak programs. The energy scale was calibrated by assigning 284.8 eV to the C1*s* peak corresponding to adventitious carbon. Electrical characterization with resistance curves as a function of temperature R(T) was carried out studying the metal-insulator transition behavior of the VO_2 compound and of the BFO/VO_2 system, additional measurements of current versus voltage, I-V, were made by the method of Van der Paw or method of the four points and finally the results obtained were correlated.

3. Results and discussion

3.1 Profilometry and AFM studies

Preprints (www.preprints.org) | NOT PEER-REVIEWED | Posted: 30 June 2022 doi:10.20944/preprints202206.0416.v1

Figures 1 and **2** show profilometry measurements of the VO_2/Al_2O_3 thin films. In **Figure 1**, the approximate thickness of 77.5 nm provided by the step height parameter (StpHt) indicates a growth rate of 1.3 nm per minute. Instead, in the 3D profile uniform height regions can be seen on moving away from the step, denoting an ordered growth. In the case of BFO/$SrTiO_3$ thin films, see **Figures 3** and **4**, the thickness of the BFO films was 106.5 nm, on average, which indicates a growth rate of 2.4 nm per minute under the BFO growth parameters. In these films the step is more marked, possibly because the mask was much better adhered and did not allow diffusion between film and mask. Although the maximum height Z is lower than in the VO_2 films, there is less homogeneity and there are several zones with different heights.

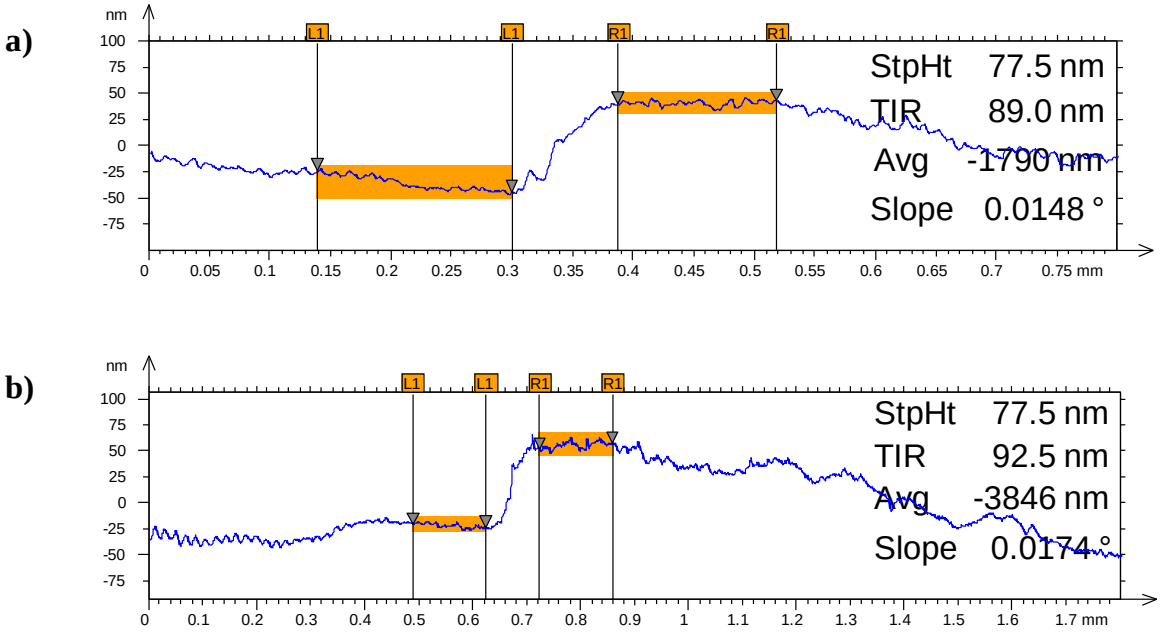

Figure 1. a,b) Profilometry measurements at two different points of thin films of VO_2 on Al_2O_3.

Preprints (www.preprints.org) | NOT PEER-REVIEWED | Posted: 30 June 2022 doi:10.20944/preprints202206.0416.v1

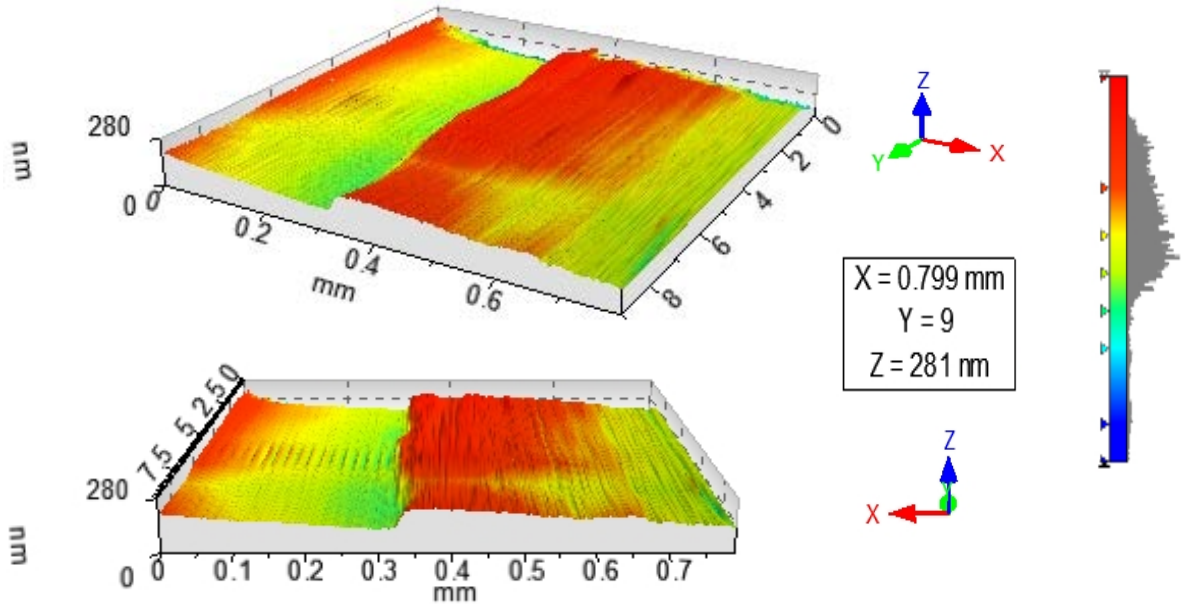

Figure 2. 3D image obtained by profilometry of the surface of thin films of VO_2 on Al_2O_3.

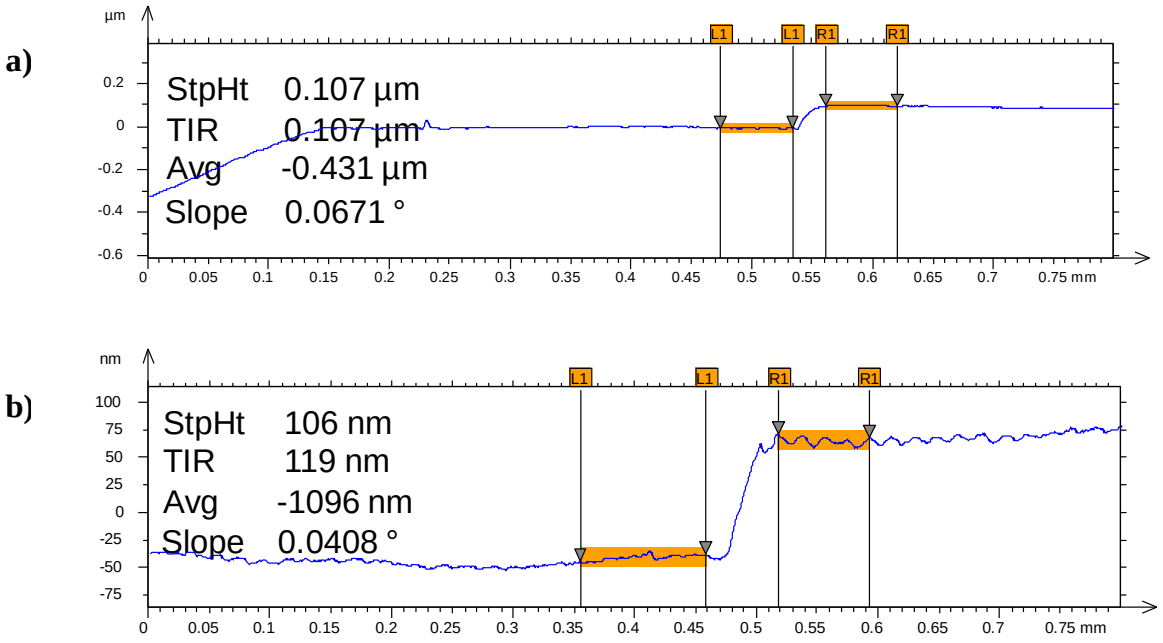

Figure 3. a,b) Profilometry measurements at two different points of thin films of BFO on $SrTiO_3$.

Preprints (www.preprints.org) | NOT PEER-REVIEWED | Posted: 30 June 2022 doi:10.20944/preprints202206.0416.v1

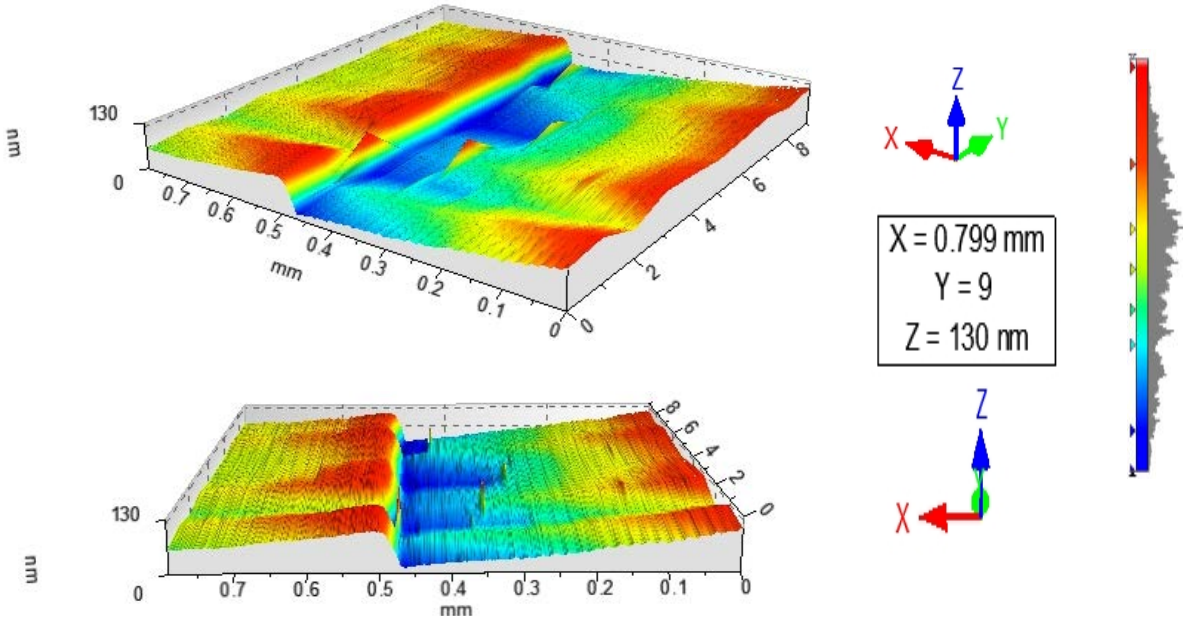

Figure 4. 3D image obtained by profilometry of the surface of thin films of BFO on $SrTiO_3$.

Surface roughness plays an important role on the effects generated at the interface of the films. For example, in multiferroics systems the roughness can influence the magnetic and electrical properties of these films. Therefore, the surface of the individual layers and the BFO/VO_2 heterostructures is analyzed by AFM, see **Figures 5, 6,** and **7** [18]. Good granular ordering and RMS roughnesses between 1 and 5 nm were observed for the individual layers and between 6 and 18 nm for the bilayers, see **Figure 8.** The films exhibited a dense morphology, a continuous surface, and a fine grain microstructure without cracks. The samples with greater presence of high peaks are due to the agglomerations of particles that appear in longer growth times, in the same way the grain size for long growth times is smaller and with more uniformity.

Figure 5 shows the image of the surface scan of a section of 1 x 1 μm^2 and a histogram with the average grain size, which was 26 nm for a monolayer film of VO_2. In these monolayers, surface roughness and grain size increase with deposition time. However, **Figure 6** reveals that the grain size of the BFO films is highly homogeneous. No large peaks or valleys were observed. The average grain size is 20 nm and the roughness does not seem to increase significantly with the increase in thickness.

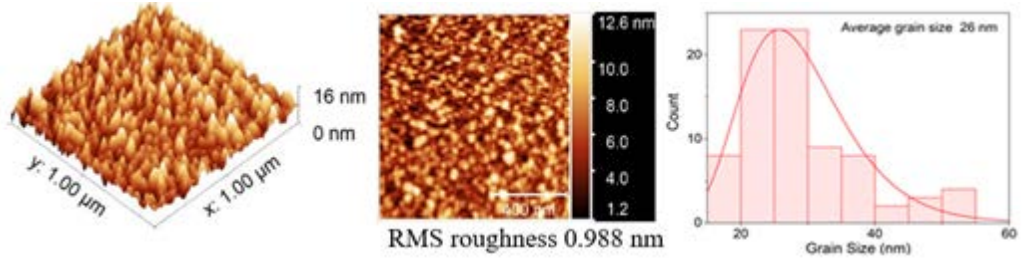

Figure 5. AFM measurements and average grain size for VO_2 thin films

Preprints (www.preprints.org) | NOT PEER-REVIEWED | Posted: 30 June 2022 doi:10.20944/preprints202206.0416.v1

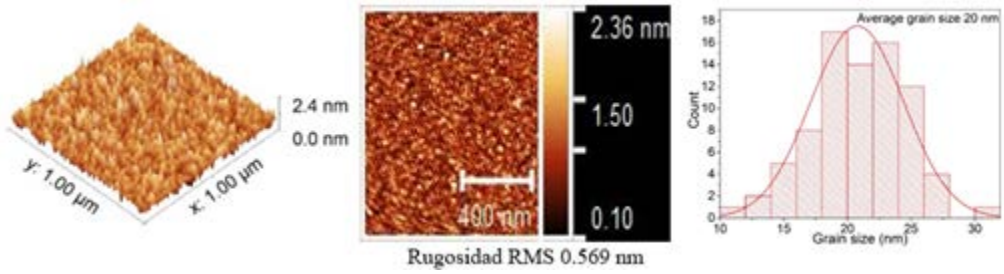

Figure 6. AFM measurements and average grain size for BFO thin films

Figure 7 shows that the grain size of the BFO/VO_2 films is 63 nm and increases to 67 nm when the BFO layer is 30 and 60 nm, respectively. This could be because the grain geometry is more elongated in the bilayers of 30 nm and roughness 10.10 nm than with bilayer of 60 nm and roughness 16.62 nm. This shows us a more elongated grain geometry in the bilayers, especially the bilayers with greater thicknesses. This elongation in the grains influences the roughness which increases with respect to the individual layers, this translates into greater growth by islands and agglomerations of scattered particles with greater height.

Thus, is observed in the literature reports that these films grow layer by layer following the structure of terraces and substrate steps [19]-[23]. Atoms reaching the surface of the substrate are placed in the middle of the step and, from there, the structure grows in 2D form until complete coalescence between the different levels of layer. The atoms deposited on the substrate are more strongly attached to the next layer and so on. Growth with a larger and not so homogeneous grain size can be seen for the top layer of BFO/VO_2/Al_2O_3 with respect to the individual layers [19]. A degree of organization and absence of cracks is observed, indicating good diffusion and coupling between the BFO, VO_2 and substrate layers. These characteristics seen in the films contribute to create additional stress that increases with thickness, favoring the formation of islands in the next layer to be deposited. This stress can determine a shift in the critical transition temperature of VO_2 and therefore in the bilayer [20]–[22].

Preprints (www.preprints.org) | NOT PEER-REVIEWED | Posted: 30 June 2022 doi:10.20944/preprints202206.0416.v1

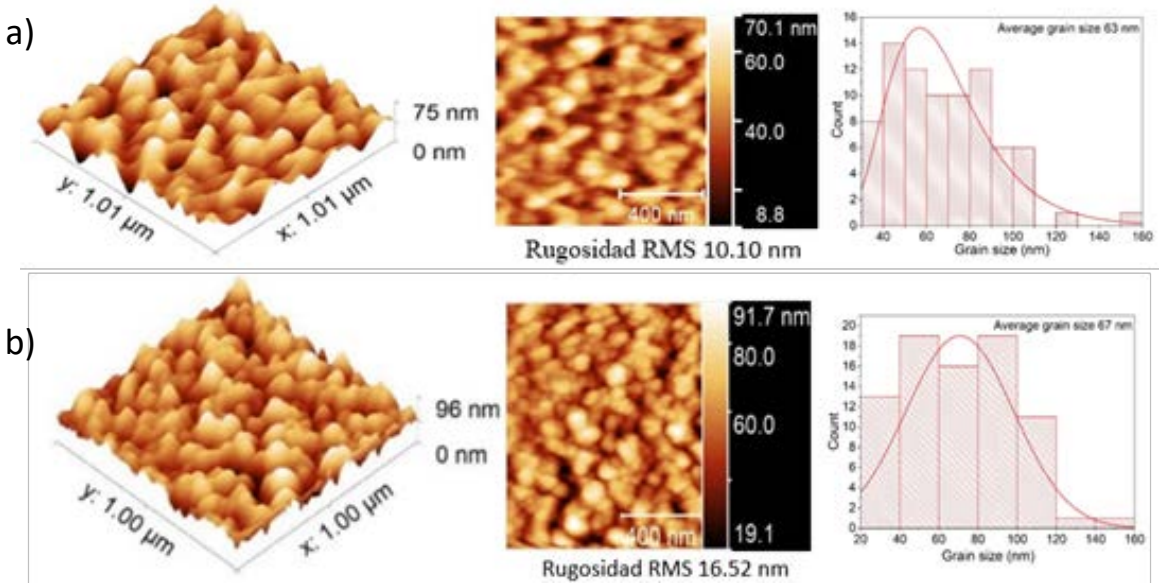

Figure 7. AFM measurements and average grain size for BFO/VO_2 thin films with BFO layer of a) 30 nm and b) 60 nm

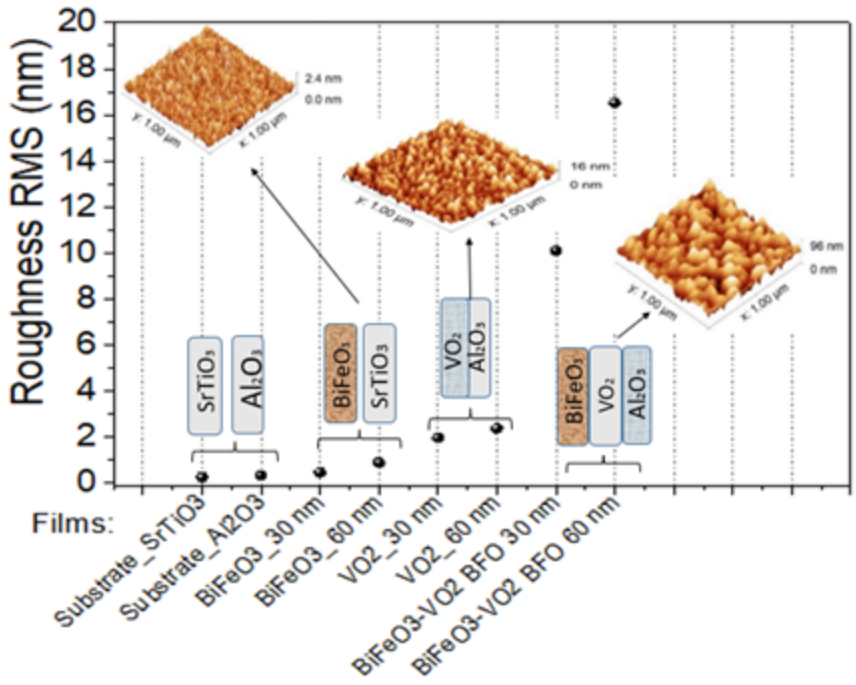

Figure 8. Roughness of films based on BFO and VO_2

Figure 8 presents a summary of the roughness of the grown films. A semi-exponential upward trend can be observed, showing us how roughness increases in these films as the thickness and number of layers of these two thin-film materials increase.

3.2 Chemical states

Preprints (www.preprints.org) | NOT PEER-REVIEWED | Posted: 30 June 2022 doi:10.20944/preprints202206.0416.v1

The chemical studies have been carried out through XPS analysis to detect the chemical states in these thin films. The analysis of surfaces by XPS is a very valuable resource when determining both quantitatively and qualitatively the composition and chemical state of surfaces. However, the analysis by this technique of first-row transition metals and their oxides and hydroxyls is a challenge due to the complexity of their *2p* spectra resulting from asymmetric peaks, the complex division of multiplets and the uncertain and overlapping union of energies [24].

XPS measurements are presented for 4 samples, 2 monolayers (VO_2/Al_2O_3 and $BFO/SrTiO_3$) and 2 bilayers ($BFO/VO_2/Al_2O_3$, with BFO layer of 30 and 60 nm), respectively. These measurements were made in broad spectrum and high-resolution and are shown in **Figures 9** to **12**. All spectra were corrected by the binding energy of carbon at 284.8 eV and adjusted with mixed Lorentzian and Gaussian curves. The Mo signal is from the sample holder.

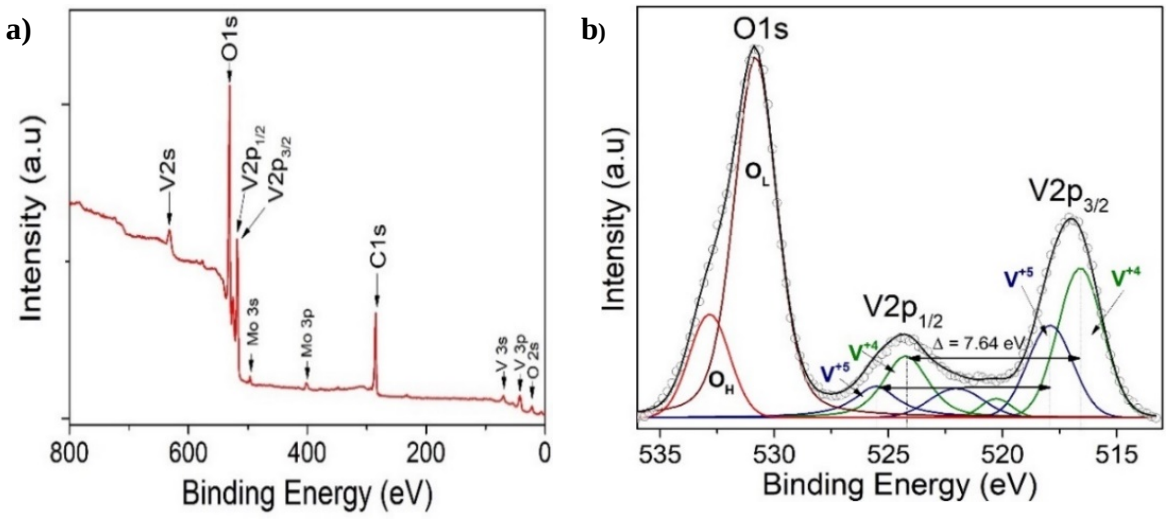

Figure 9. Broad (a) and high-resolution (b) XPS spectrum of VO_2 monolayer

Figure 9 shows the spectra of VO_2/Al_2O_3 monolayer. **Figure 9a)** can be seen the absence of impurity peaks except for molybdenum (Mo) coming from the sample holder used. However, a high-resolution spectrum, **Figure 9b)**, the respective curve adjustment was obtained for V^{+4} peaks (516.6 eV and 524.24 eV), V^{+5} peaks (517.94 eV and 525.58 eV), O_L peak (530.84 eV), and O_H peak (532.81 eV), respectively. Here, O_L and O_H peaks correspond to the bonds of oxygen with hydrogen and the crystal lattice of the compound studied and indicates that the films are very susceptible to oxidation in the environment. In addition, a distance between the vanadium doublet of 7.64 eV typical of vanadium oxides is observed, and it is evident that the predominant oxidation state is V^{+4}, which corresponds to VO_2. On the other hand, **Figure 10** shows the spectra of $BFO/SrTiO_3$ monolayer. It is observed signals from bismuth, iron, oxygen, and molybdenum (from sample

Preprints (www.preprints.org) | NOT PEER-REVIEWED | Posted: 30 June 2022 doi:10.20944/preprints202206.0416.v1

holder), see **Figure 10a)**. However, using high-resolution is possible to determine the composition in the thin film (**Figures 10 b)-d)**). It is observed signals from Fe(2*p*) doublet (at 710.02 and 723.62 eV) and Bi(4*f*) doublet (at 156.84 and 162.15 eV), including metallic Bi. Their binding energies differences for each is 13.6 eV and 5.31 eV, respectively, which constitutes a response of iron oxides and bismuth oxides. On the other hand, the high-resolution spectra of oxygen (O1*s*, see **Figure 10d)**) show the presence of the oxides of the lattice (metallic oxides, O_L) and hydroxyl oxygen (O_H) in the thin films. Therefore, it is clearly observed that the predominant oxidation states are Fe^{3+} and Bi^{3+} corresponding to the structure of $BiFeO_3$.

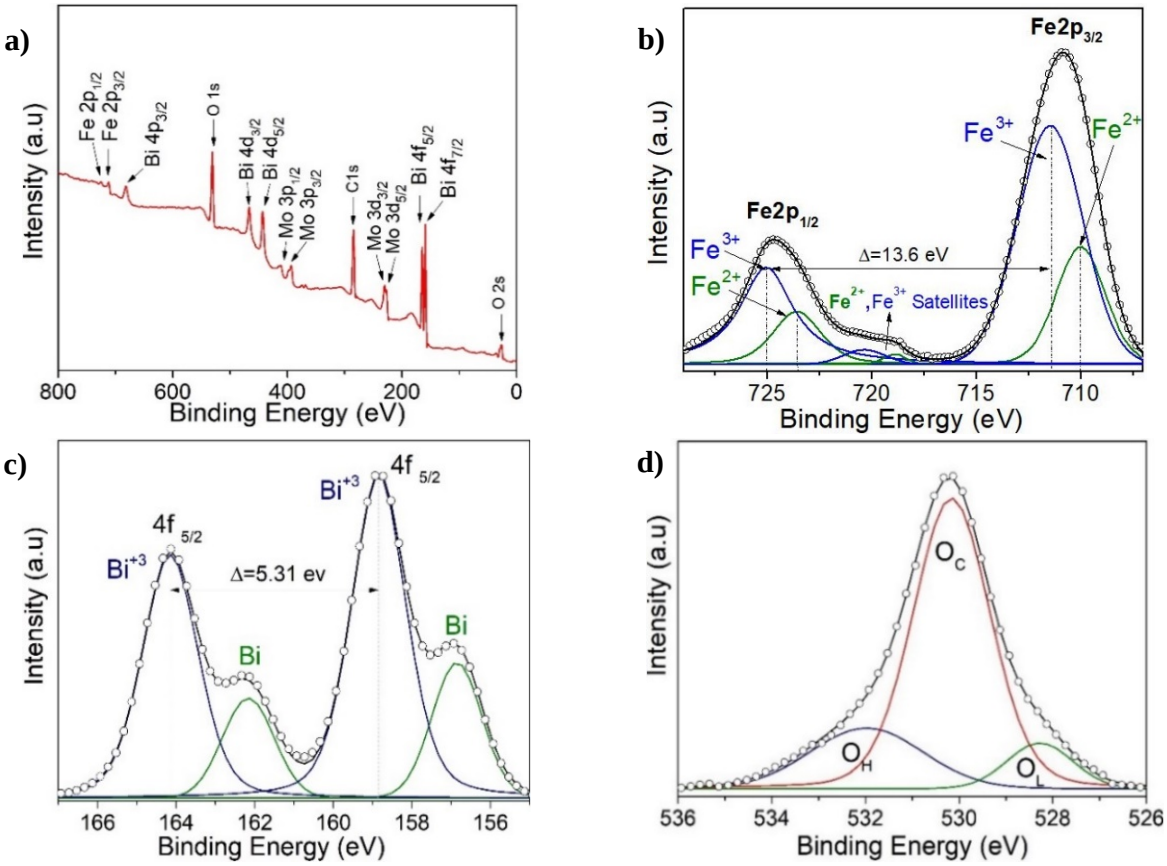

Figure 10. Broad (a) and high-resolution (b, c, d) XPS spectra of BFO/$SrTiO_3$ monolayer

For the bilayer thin films, **Figure 11 and Figure 12**, we can observe that the Fe(2*p*) doublet and Bi(4*f*) doublet binding energies difference of 13.6 eV and 5.31 eV are maintained. Therefore, the BFO thin films with layer of 30 nm exhibits more oxidation states as well as a shift towards higher binding energies. However, an ion bombardment revealed that the amount of Fe^{3+} increases in the BFO thin films, unlike the surface where there was a higher presence of the Fe^{2+} oxidation state. In the bilayers, there was a small displacement of the maximums towards higher values of binding energy, however, this did not increase the number of oxidation

Preprints (www.preprints.org) | NOT PEER-REVIEWED | Posted: 30 June 2022 doi:10.20944/preprints202206.0416.v1

states and it can be noted that at less layer, Fe^{3+} increases in proportion. On the other hand, it is evident that Bi^{3+} is very predominant in both monolayers and bilayers. Instead, there are an increase in the contribution of the oxides of the lattice (metallic oxides, O_L) for the bilayers, which is a good indication that the surface area is more homogeneous and that there is less contamination. In addition, hydroxyl oxygen (O_H) increases in the thin films with lower growth power and in the eroded sample, which may suggest that these thin films could be more photocatalytic.

Figure 13 shows a summary of the atomic percentages of the thin films analyzed in this work. It is observed that the VO_2 films most indicated to be coupled with the BFO films are those with 60 min of growth, since they have a higher percentage of vanadium on the surface and presented a higher proportion of V^{4+}. On the other hand, the most suitable BFO films to couple in the bilayer with VO_2 are those with a BFO layer of 30 nm, because they show iron with a higher atomic percentage in the surface area and a higher Fe^{3+} ratio.

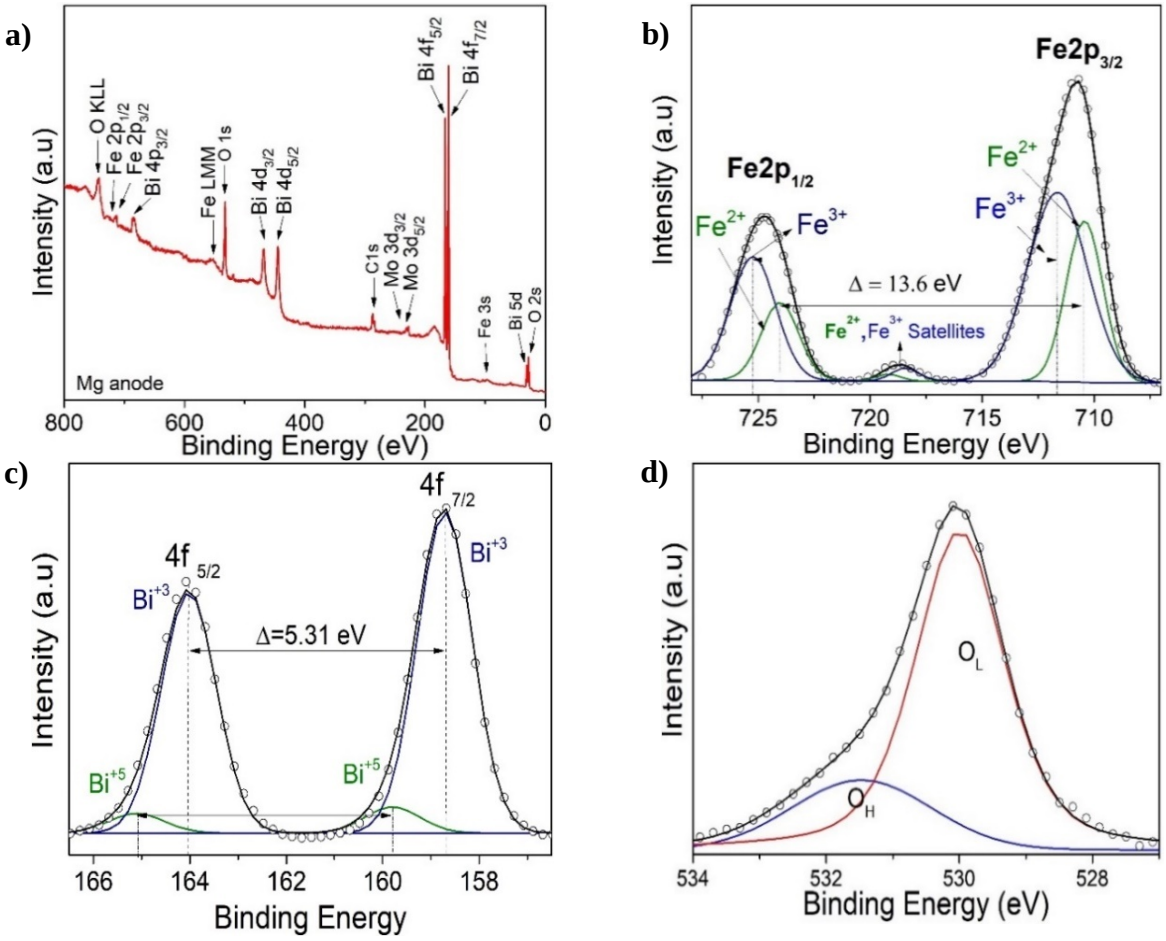

Figure 11. Broad (a) and high-resolution (b, c, d) XPS spectra of BFO/VO_2 bilayer with BFO layer of 30 nm

Preprints (www.preprints.org) | NOT PEER-REVIEWED | Posted: 30 June 2022 doi:10.20944/preprints202206.0416.v1

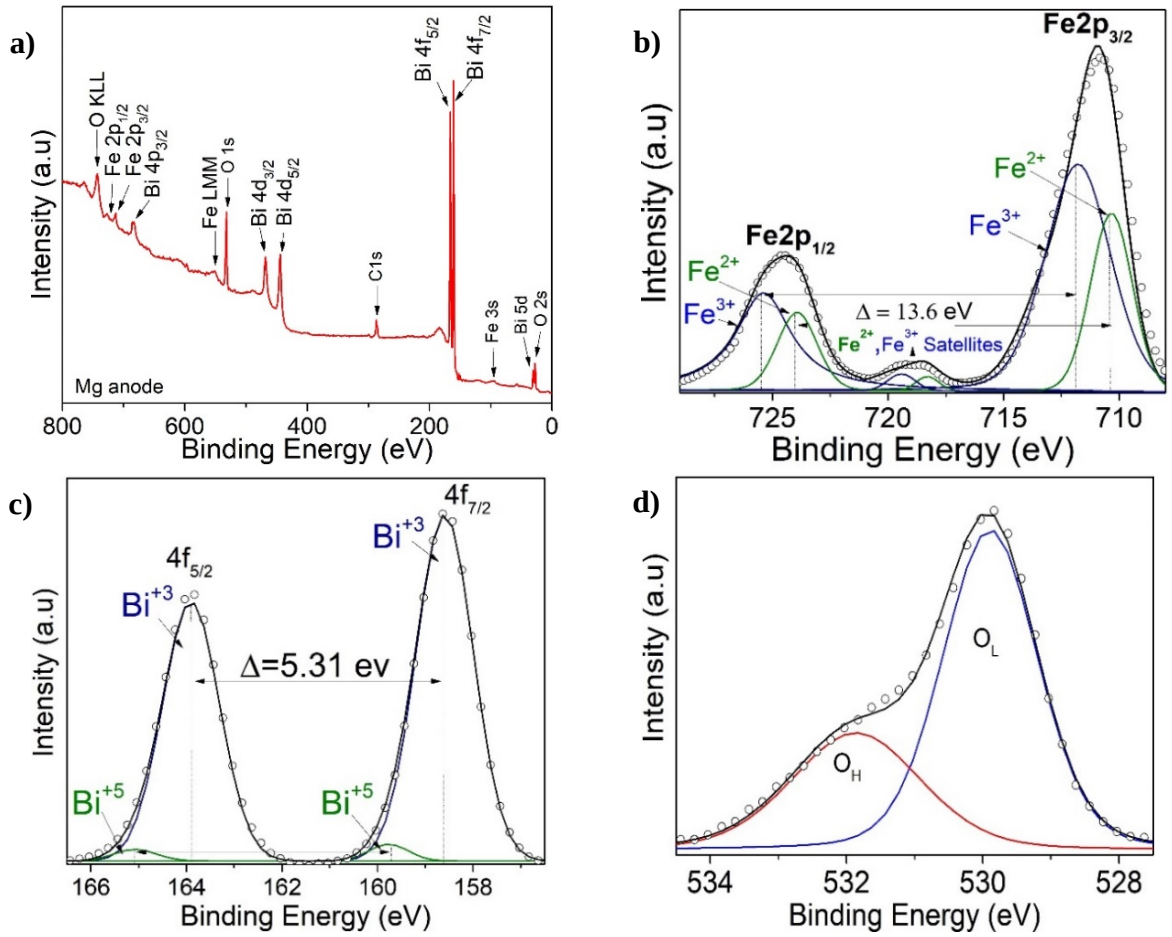

Figure 12. Broad (a) and high-resolution (b, c, d) XPS spectra of BFO/VO_2 bilayer with BFO layer of 60 nm

Finally, it should be noted that growing this type of film in bilayer without previous antecedents constituted a challenge, not only because of the coupling of their crystalline structures before and after the VO_2 transition temperature, but also because the upper layer (BFO) is grown at a higher temperature than the lower VO_2 layer and even its annealing temperature at 470 °C. This has therefore deoxidation of the VO_2 film turning metallic and losing its metal insulator transitions (MIT), which is not desirable, since coupling with a material that presents a structural phase transition is essential to generating a new line of applications and studies of the physical properties of these bilayers. Therefore, the VO_2 films were carefully over-oxidized, anticipating these losses when the upper BFO film grew and in this way a growth methodology of these bilayers was obtained.

Preprints (www.preprints.org) | NOT PEER-REVIEWED | Posted: 30 June 2022 doi:10.20944/preprints202206.0416.v1

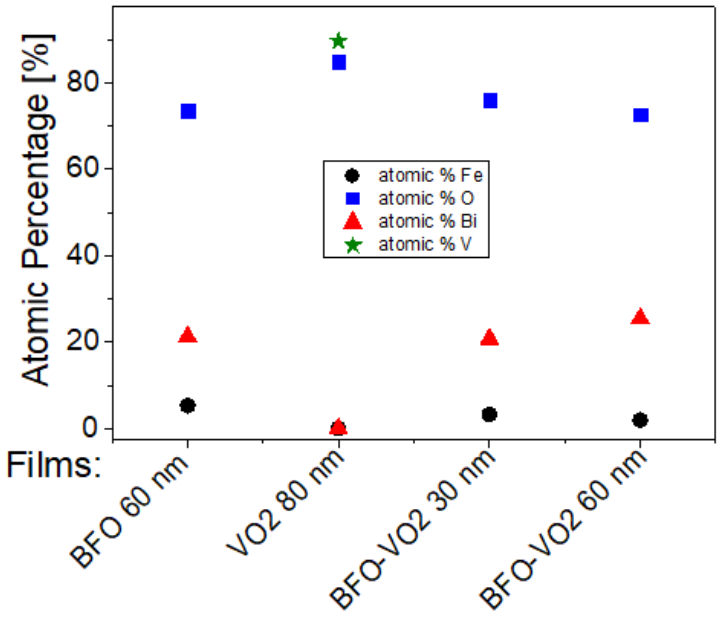

Figure 13. Atomic percentages on the surface of the selected films.

3.3 Electrical characterization

One of the best indications of the good coupling in the bilayers based on BFO and VO_2, is that these also present hysteresis curves with a decrease of several orders of magnitude of electrical resistance in a fairly short time, see **Figure 14 left)**, even so, there is a leftward shift in the transition temperature with respect to the 340 K of VO_2 , this lower value (around ~325 K) can be caused by the increase in interfacial tension in VO_2, since, there are studies such as the reported in Refs [20] and [25], which show us that there is a relationship between the increase in the tension of the crystal lattice in VO_2 and the decrease in critical temperature. This result corroborates the XRD analysis that show tensions in its crystal lattice, this would be, not only with the substrate of Al_2O_3 but also with the film on it (BFO). Additionally, this possibly contributes to increase the voltage of the lattice in the VO_2 and therefore to decrease the transition temperature.

The electrical properties of the BFO/VO_2/Al_2O_3 heterostructures are shown in **Figure 14**. A well-defined MIT with a resistance change of two and three orders of magnitude (ΔR ~100 and ~1000) can be seen in a) and b) with an T_{MIT} between ~ 322 and 327 K (hysteresis width between $\Delta H \approx 4$ and 3 K) for the 30 and 60 nm bilayers respectively. T_{MIT} is estimated by the well-known expression $T_{MIT} = ½(T_c - T_h)$. Here, $(T_c - T_h)$ represent the transition temperatures at the center of the derived curve (d[log(R)]/dT) during the cooling and heating procedure, respectively (inset in **Figure 14 right)**). The observation of an MIT, which improves the conductivity of the studied system, confirms the presence of the VO_2(M) phase in the lower film. Here, it should be noted that the VO_2(B) phase exhibits neither MIT nor thermal hysteresis phenomena [26]. The resistance of VO_2(B) decreases exponentially with increasing temperature [27]. It is striking that the measured

Preprints (www.preprints.org) | NOT PEER-REVIEWED | Posted: 30 June 2022 doi:10.20944/preprints202206.0416.v1

T_{MIT} of the polycrystalline film VO_2 in the heterostructure is relatively low compared to that reported for individual crystals or epitaxial thin films [28] . This finding, along with the observed resistance change of several orders of magnitude, are in agree with the results reported for polycrystalline VO_2 thin films [29], [30].

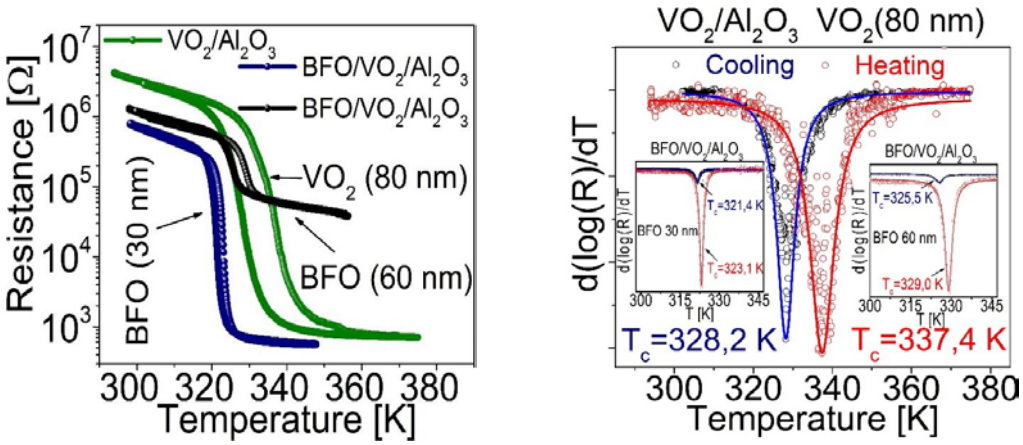

Figure 14. left) Resistance curves as a function of temperature for VO_2/Al_2O_3 (VO_2 80 nm), $BFO/VO_2/Al_2O_3$ (BFO layer of 30 nm) and $BFO/VO_2/Al_2O_3$ (BFO layer of 60 nm), right) derived from electrical resistance as a function of temperature, for the films obtained.

It is worth mentioning that the growth of polycrystalline thin films of VO_2 with reduced T_{MIT} is technologically interesting and constitutes a current research topic in solid state physics [31]. Although the T_{MIT} of the polycrystalline thin film VO_2 can be effectively adjusted and various approaches have been adopted to explain the origin of the reduced T_{MIT}, there is no consensus on this matter. Therefore, the true physical mechanism behind the reduction in the T_{MIT} value of polycrystalline VO_2 thin films remains an open question.

Although understanding the phase transition in thin-film VO_2 is challenging, it is probably related to a network distortion process. In a simplified image, it has been argued that a charge density wave along the c-axis of rutile [32], with the wave vector 2cR, forms during transition. As a result, the unit cell along the c-axis is duplicated, generating a periodic distortion of the network in this direction. A slight rotation of the dimers with respect to the c-axis has also been verified [32]. As for the phase transition of VO_2 polycrystalline films, it is evident that the phase transition in this case is easier than that of VO_2 monocrystals [21]. The main feature of VO_2 polycrystalline films is the deformation compatibility between differently oriented grains. Therefore, it is to be expected that grains oriented along specific directions may have irregular distortions of the network.

To finish with the characterizations carried out, it was decided to study I-V curves to analyze the electrical behavior of the bilayer thin film with BFO layer of 30 nm, as a first approximation to future studies of these bilayers in functional applications for storage devices, such as memresistors. The bilayer thin film with BFO

 doi:10.20944/preprints202206.0416.v1

layer of 30 nm was chosen because it was the one that, in percentage, varied its electrical and magnetic responses more compared to the MIT of VO_2, therefore, the film that has the greatest potential to work with nanotechnological applications or prototypes.

Figure 15 shows the I-V curves of BFO/Al_2O_3 (BFO layer of 30 nm) varying voltage from 0 V to 200 V at different temperatures (**Figure 15 (up)**) and from -200V to 200V at a temperature of 320 K (**Figure 15 (down)**). Here, it is evident how the film progressively goes from having an ohmic behavior at room temperature to having a hysteresis cycle typical of resistive memories, which has a maximum width of ~ 20 V and as the temperature decreases this hysteresis cycle closes.

Preprints (www.preprints.org) | NOT PEER-REVIEWED | Posted: 30 June 2022 doi:10.20944/preprints202206.0416.v1

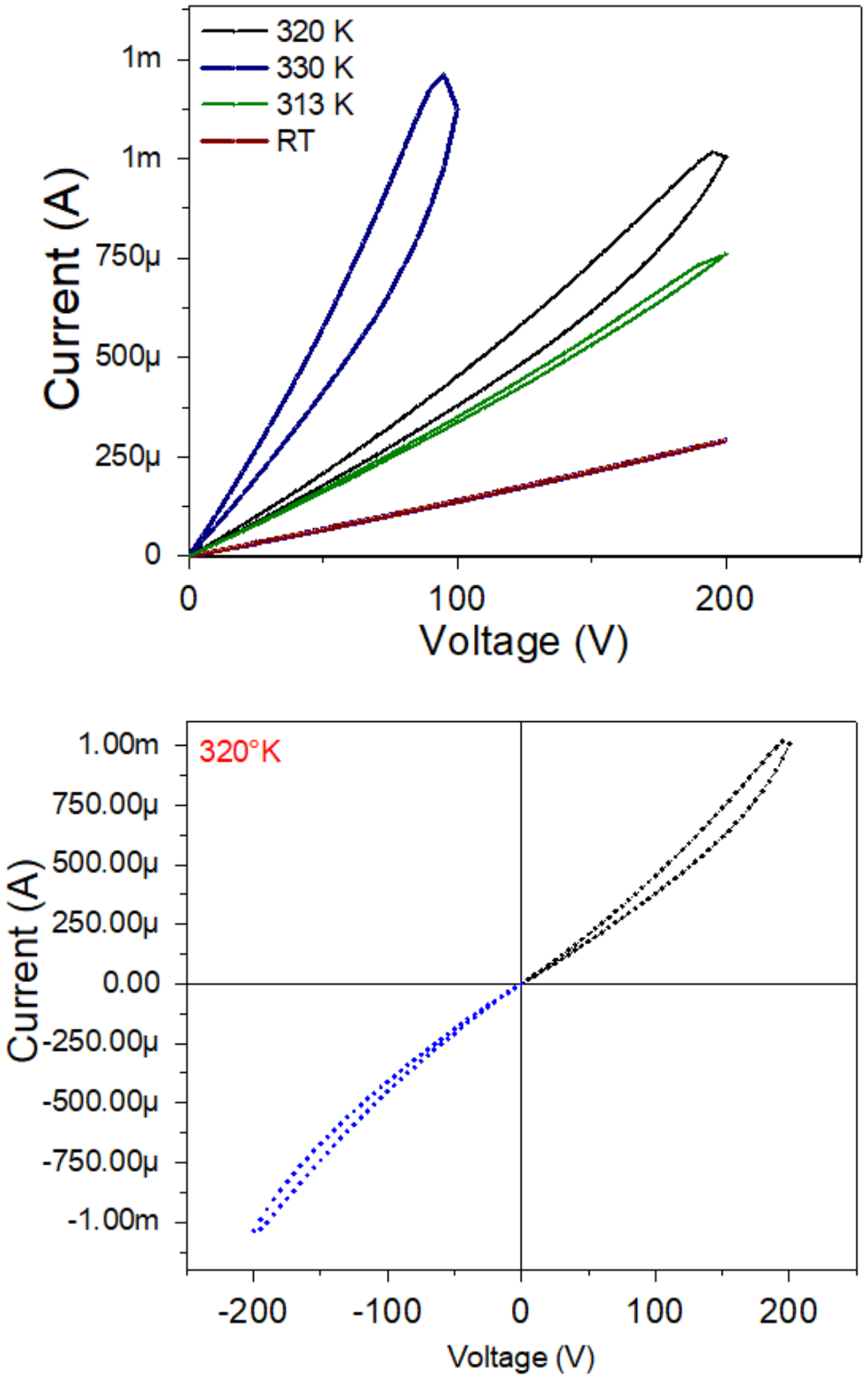

Figure 15. I-V curves for a BFO/VO_2/Al_2O_3 bilayer, with BFO layer of 30 nm, with different temperatures (up), and at 320 K with positive and negative voltage values (down).

Studying more thoroughly the I-V of the bilayer at 320 K, we can observe a difference in the symmetry of the resistive cycle with positive and negative voltages, however, the negative voltage cycle is closed more, an

 doi:10.20944/preprints202206.0416.v1

effect that agrees with what is reported in Refs. [33] and [34]. Here, it is denoted that it is a typical behavior of these memresistor materials, that they change their response with each measurement.

On the other hand, effects such as magnetoelectric coupling and its behavior at different fields and with temperatures before and after the transition would be a next step for the study of these heterostructures with high mismatch and FE/ AF/MIT coupling.

4. CONCLUSIONS

It was possible to obtain the growth parameters for films based on BFO and VO_2, together with a methodology that allows obtaining a good coupling between films and the desired oxidation states of vanadium, bismuth, and iron. BFO and VO_2 monolayers were obtained with ordered growth, good adherence, roughness (between 0.2 and 2.3 nm), and grain size (between 20 and 32 nm). In addition, an ordered growth without cracks is evidenced. AFM measurements show differences in the topography of the individual layers and bilayers, a change in the average grain diameter from 20 nm to 67 nm and a change in roughness from 0.2 nm to almost 16 nm in BFO/VO_2 bilayers.

AFM measurements show differences in the topography of individual monolayers and bilayers, a change in average grain diameter from 20 nm to 67 nm was observed, and a change in roughness from 0.2 nm to nearly 16 nm was observed in BFO/VO_2 bilayers. In addition, an orderly growth without cracks (AFM) is evident. The homogeneity observed in the films with the best results will possibly contribute to obtaining good results in characterizations of current, voltage, resistance and behavior against electric and magnetic fields. It was observed by means of XPS that the predominant oxidation state in the individual and bilayer thin films is VO_2. However, there is also a presence in the films of the V_2O_5 phase. The BFO and BFO/VO_2/Al_2O_3 films show the presented $BiFeO_3$ as the predominant phase.

Furthermore, thin films show a structural phase change with resistance change of several orders of magnitude, both for monolayers and for bilayers. Also, hysteresis loops are presented here, which is an excellent indication to work these films in memresistor and solar cells.

Author Contributions: All author participated in Conceptualization, methodology, research, analysis, writing and editing the original draft. All authors have read and agreed to the published version of the manuscript.

Funding: This research was funded by *Sistema General de Regalías*, through project with BPIN 2018000100092

Acknowledgments: We are very grateful to the Alliance of the Pacific and Minciencias (Colfuturo 727-2015 and SGR BPIN2018000100092). This work is supported by Universidad del Valle (Hard Coatings and Industrial Applications (RDAI) laboratory and Strengthening of Centers and Institutes) and Universidad de Chile. We are especially grateful to Colin McLachlan for suggestions related to the English text.

Conflicts of Interest

There are no conflicts to declare

References

[1] W. Mao *et al.*, "Combined experimental and theoretical investigation on modulation of multiferroic properties in $BiFeO_3$ ceramics induced by Dy and transition metals co-doping," *Journal of Alloys and Compounds*, vol. 784, pp. 117–124, May 2019, doi: 10.1016/j.jallcom.2018.12.381.

[2] M. Kumar and K. L. Yadav, "Magnetic field induced phase transition in multiferroic BiFe1−xTixO3 ceramics prepared by rapid liquid phase sintering," *Applied Physics Letters*, vol. 91, no. 11, p. 112911, Sep. 2007, doi: 10.1063/1.2784179.

[3] A. M. Kadomtseva, Yu. F. Popov, A. P. Pyatakov, G. P. Vorob'ev, A. K. Zvezdin, and D. Viehland, "Phase transitions in multiferroic $BiFeO_3$ crystals, thin-layers, and ceramics: enduring potential for a single phase, room-temperature magnetoelectric 'holy grail,'" *Phase Transitions*, vol. 79, no. 12, pp. 1019–1042, Dec. 2006, doi: 10.1080/01411590601067235.

[4] F. Zavaliche *et al.*, "Multiferroic $BiFeO_3$ films: domain structure and polarization dynamics," *Phase Transitions*, vol. 79, no. 12, pp. 991–1017, Dec. 2006, doi: 10.1080/01411590601067144.

[5] L. Yin and W. Mi, "Progress in $BiFeO_3$-based heterostructures: Materials, properties and applications," *Nanoscale*, vol. 12, no. 2, pp. 477–523, Jan. 2020, doi: 10.1039/c9nr08800h.

[6] J. Lauzier, L. Sutton, and J. de la Venta, "Magnetic irreversibility in VO_2 /Ni bilayers," *Journal of Physics: Condensed Matter*, vol. 30, no. 37, p. 374004, Sep. 2018, doi: 10.1088/1361-648X/aad5af.

[7] L. Sutton *et al.*, "Effects of W Doping in VO_2 on the Magnetic Properties of VO_2/Ni Heterostructures," *Journal of Superconductivity and Novel Magnetism*, vol. 33, no. 8, pp. 2493–2499, Aug. 2020, doi: 10.1007/s10948-020-05504-3.

[8] N. A. Spaldin and M. Fiebig, "The Renaissance of Magnetoelectric Multiferroics," *Science (1979)*, vol. 309, no. 5733, pp. 391–392, Jul. 2005, doi: 10.1126/science.1113357.

[9] J. de la Venta, S. Wang, J. G. Ramirez, and I. K. Schuller, "Control of magnetism across metal to insulator transitions," *Applied Physics Letters*, vol. 102, no. 12, p. 122404, Mar. 2013, doi: 10.1063/1.4798293.

[10] J. de la Venta, S. Wang, T. Saerbeck, J. G. Ramírez, I. Valmianski, and I. K. Schuller, "Coercivity enhancement in V_2O_3 /Ni bilayers driven by nanoscale phase coexistence," *Applied Physics Letters*, vol. 104, no. 6, p. 062410, Feb. 2014, doi: 10.1063/1.4865587.

[11] T. Saerbeck *et al.*, "Coupling of magnetism and structural phase transitions by interfacial strain," *Journal of Materials Research*, vol. 29, no. 20, pp. 2353–2365, Oct. 2014, doi: 10.1557/jmr.2014.253.

[12] L. Yin and W. Mi, "Progress in $BiFeO_3$ -based heterostructures: materials, properties and applications," *Nanoscale*, vol. 12, no. 2, pp. 477–523, 2020, doi: 10.1039/C9NR08800H.

[13] M. K. Lee, T. K. Nath, C. B. Eom, M. C. Smoak, and F. Tsui, "Strain modification of epitaxial perovskite oxide thin films using structural transitions of ferroelectric $BaTiO_3$ substrate," *Applied Physics Letters*, vol. 77, no. 22, pp. 3547–3549, Nov. 2000, doi: 10.1063/1.1328762.

[14] N. v. Burbure, P. A. Salvador, and G. S. Rohrer, "Orientation and Phase Relationships between Titania Films and Polycrystalline BaTiO3 Substrates as Determined by Electron Backscatter Diffraction Mapping," *Journal of the American Ceramic Society*, vol. 93, no. 9, pp. 2530–2533, Jun. 2010, doi: 10.1111/j.1551-2916.2010.03878.x.

[15] H.-J. Feng, "Photovoltaic and magnetic properties of $BiFeO_3$/TiO_2 heterostructures under epitaxial strain and an electric field," *Materials Chemistry and Physics*, vol. 153, pp. 405–409, Mar. 2015, doi: 10.1016/j.matchemphys.2015.01.034.

[16] A. Sarkar, G. G. Khan, A. Chaudhuri, A. Das, and K. Mandal, "Multifunctional $BiFeO_3$/TiO_2 nano-heterostructure: Photo-ferroelectricity, rectifying transport, and nonvolatile resistive switching property," *Applied Physics Letters*, vol. 108, no. 3, p. 033112, Jan. 2016, doi: 10.1063/1.4940118.

[17] Y. Zhang, A. M. Schultz, L. Li, H. Chien, P. A. Salvador, and G. S. Rohrer, "Combinatorial substrate epitaxy: A high-throughput method for determining phase and orientation relationships and its application to $BiFeO_3/TiO_2$ heterostructures," *Acta Materialia*, vol. 60, no. 19, pp. 6486–6493, Nov. 2012, doi: 10.1016/j.actamat.2012.07.060.

[18] Q. Xu, Y. Sheng, X. Xue, X. Yuan, Z. Wen, and J. Du, "Exchange bias in $BiFeO_3/La_{0.67}Sr_{0.33}MnO_3$ bilayers," *Japanese Journal of Applied Physics*, vol. 53, no. 8S3, p. 08NM01, Aug. 2014, doi: 10.7567/JJAP.53.08NM01.

[19] L. Eckertová, "Mechanism of Film Formation," in *Physics of Thin Films*, Boston, MA: Springer US, 1977, pp. 72–114. doi: 10.1007/978-1-4615-7589-4_4.

[20] C. Chen *et al.*, "Influence of defects on structural and electrical properties of VO_2 thin films," *Journal of Applied Physics*, vol. 110, no. 2, p. 023707, Jul. 2011, doi: 10.1063/1.3609084.

[21] T. Lin, L. Wang, X. Wang, Y. Zhang, and Y. Yu, "Influence of lattice distortion on phase transition properties of polycrystalline VO2 thin film," *Applied Surface Science*, vol. 379, pp. 179–185, Aug. 2016, doi: 10.1016/j.apsusc.2016.04.007.

[22] P. A. Cox, "The Electronic Structure of Transition Metal Oxides and Chalcogenides," 1996, pp. 255–270. doi: 10.1007/978-1-4613-1149-2_15.

[23] K. Oura, M. Katayama, A. v. Zotov, V. G. Lifshits, and A. A. Saranin, "Growth of Thin Films," Heidelberg: Springer., Berlin: Advanced Texts in Physics, 2003, pp. 357–387. doi: 10.1007/978-3-662-05179-5_14.

[24] M. C. Biesinger, B. P. Payne, A. P. Grosvenor, L. W. M. Lau, A. R. Gerson, and R. S. C. Smart, "Resolving surface chemical states in XPS analysis of first row transition metals, oxides and hydroxides: Cr, Mn, Fe, Co and Ni," *Applied Surface Science*, vol. 257, no. 7, pp. 2717–2730, 2011, doi: 10.1016/j.apsusc.2010.10.051.

[25] V. Théry *et al.*, "Role of thermal strain in the metal-insulator and structural phase transition of epitaxial VO_2 films," *Physical Review B*, vol. 93, no. 18, p. 184106, May 2016, doi: 10.1103/PhysRevB.93.184106.

[26] Ch. Leroux, G. Nihoul, and G. van Tendeloo, "From VO_2(B) to VO_2(R)◎: Theoretical structures of VO_2 polymorphs and in situ electron microscopy," *Physical Review B*, vol. 57, no. 9, pp. 5111–5121, Mar. 1998, doi: 10.1103/PhysRevB.57.5111.

[27] Z. Ding, Y. Cui, D. Wan, H. Luo, and Y. Gao, "High-performance thermal sensitive VO_2 (B) thin films prepared by sputtering with TiO_2 (A) buffer layer and first-principles calculations study," *RSC Advances*, vol. 7, no. 47, pp. 29496–29504, 2017, doi: 10.1039/C7RA03239K.

[28] Y. K. Dou *et al.*, "Oxidizing annealing effects on VO_2 films with different microstructures," *Applied Surface Science*, vol. 345, pp. 232–237, 2015, doi: 10.1016/j.apsusc.2015.03.044.

[29] D. Brassard, S. Fourmaux, M. Jean-Jacques, J. C. Kieffer, and M. A. el Khakani, "Grain size effect on the semiconductor-metal phase transition characteristics of magnetron-sputtered VO2 thin films," *Applied Physics Letters*, vol. 87, no. 5, p. 051910, Aug. 2005, doi: 10.1063/1.2001139.

[30] C. Ba, S. T. Bah, M. D'Auteuil, P. v. Ashrit, and R. Vallée, "Fabrication of High-Quality VO_2 Thin Films by Ion-Assisted Dual ac Magnetron Sputtering," *ACS Applied Materials & Interfaces*, vol. 5, no. 23, pp. 12520–12525, Dec. 2013, doi: 10.1021/am403807u.

[31] F. H. Chen *et al.*, "Control of the Metal–Insulator Transition in VO_2 Epitaxial Film by Modifying Carrier Density," *ACS Applied Materials & Interfaces*, vol. 7, no. 12, pp. 6875–6881, Apr. 2015, doi: 10.1021/acsami.5b00540.

[32] V. R. Morrison *et al.*, "A photoinduced metal-like phase of monoclinic VO_2 revealed by ultrafast electron diffraction," *Science (1979)*, vol. 346, no. 6208, pp. 445–448, Oct. 2014, doi: 10.1126/science.1253779.

[33] Z. Hu *et al.*, "Ferroelectric memristor based on Pt/$BiFeO_3$/Nb-doped $SrTiO_3$ heterostructure," *Applied Physics Letters*, vol. 102, no. 10, p. 102901, Mar. 2013, doi: 10.1063/1.4795145.

[34] H. Sun *et al.*, "$BiFeO_3$ -Based Flexible Ferroelectric Memristors for Neuromorphic Pattern Recognition," *ACS Applied Electronic Materials*, vol. 2, no. 4, pp. 1081–1089, Apr. 2020, doi: 10.1021/acsaelm.0c00094.